Plasma Chemistry and Plasma Processing (2019) 39:1103–1114
https://doi.org/10.1007/s11090-019-09992-7

ORIGINAL PAPER

Densities of Active Species in R/x%(N_2–5%H_2) (R = Ar or He) Microwave Flowing Afterglows

A. Ricard[1] · **J. P. Sarrette**[1]

Received: 21 January 2019 / Accepted: 11 April 2019 / Published online: 24 April 2019

Abstract

Afterglows of R/x(N_2–5%H_2) (R = Ar or He) flowing microwave discharges are characterized by optical emission spectroscopy. Absolute densities of N atoms and N_2(A) and N_2(X,v > 13) molecules and estimated densities of NH and H atoms are determined after calibration of the N atom density by NO titration. It is determined the variations of active species densities along the post-discharge tube from the early afterglow to the late afterglow region. Conditions allowing to obtain a high concentration of H-atoms in dominant N-atoms have been found in the early afterglow region of the R/x(N_2–5%H_2) mixture for x < 5%. From these densities, the destruction probabilities of the H-atoms on the afterglow quartz tube wall is found to be: $\gamma_H^{He} = (2–3) \times 10^{-4}$ and $\gamma_H^{Ar} = (3–4) \times 10^{-3}$. The interest of these results concerns the enhancement of surface nitriding by combined effects of N and H atoms inclusion in afterglow conditions.

Keywords Afterglows of Ar/N_2/H_2 and He/N_2/H_2 · Optical emission spectroscopy · N and H atoms densities · H-atom recombination probability

Introduction

Afterglows of N_2 flowing microwave discharges have previously been studied at medium gas pressures (1–20 Torr) for the sterilization of medical instruments by N-atoms [1, 2]. Recently [3, 4], it has been observed an enhanced nitriding of TiO_2 films in the flowing afterglow of N_2/2%H_2 microwave and RF plasmas, which was attributed to the presence of H and N atoms. Passivation of InGaN/GaN nanowires [5] and treatment of graphene films [6, 7] have also been studied in N_2 microwave afterglows.

In the present study, flowing afterglows produced by R/x%(N_2–5%H_2) (R = Ar or He) microwave plasmas have been studied by emission spectroscopy. Intensities emitted by the 11–7 band of the N_2 first positive system (1+) at 580 nm (I_{580}) and by the 1–0 band of the N_2 second positive system (2+) at 316 nm (I_{316}) were measured to obtain the absolute concentrations of N-atoms, N_2(A) and N_2(X,v > 13) after NO titration to calibrate the

✉ A. Ricard
ricard@laplace.univ-tlse.fr

1 LAPLACE, CNRS, INPT, UPS, Université de Toulouse, 118 route de Narbonne, 31062 Toulouse Cedex 9, France

N-atom density. From these measurements, NH and H-atom densities have been estimated by choosing the appropriated kinetic reactions at the origin of the NH 336 nm emission.

Experimental Set-Up

The used experimental setup is reported in Fig. 1 [1, 2, 8–10].

Ar/N_2 and He/N_2 microwave discharges are produced by a surfatron cavity operating at 2.45 GHz. In these mixtures, the plasma length was found to extend between 2 and 20 cm after the surfatron gap, depending on the N_2 amount and on the HF power.

With a quartz discharge tube of 5 mm i.d. and 20 cm in length, connected to a bent post-discharge tube of 18 mm i.d. and 50 cm in length, the residence time of the afterglow at z = 3 cm after the beginning of the 18 mm post-discharge tube is 10^{-3} s.

A pre-mixed N_2–5%H_2 gas can be introduced instead of N_2 to produce NH radicals and H-atoms in addition to the N_2 active species.

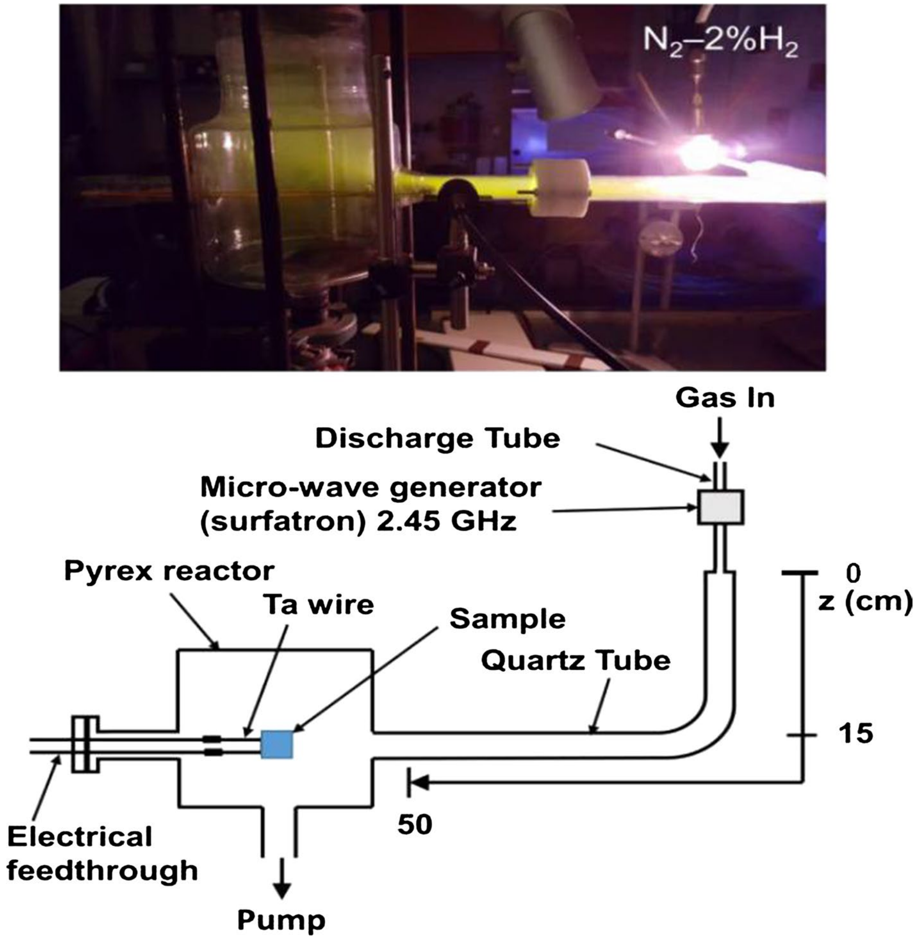

Fig. 1 Photo and scheme of the microwave flowing afterglow experimental setup

In a previous work [11], first results were presented for the same R/x(N_2–5%H_2) (R = Ar or He) gas mixtures with x ≥ 20%. The present paper focuses on early afterglow conditions (z = 3 cm) and low N_2–5%H_2 percentages (x = 2–10%).

Constant operating conditions were used, with a total gas flow rate Q_{total} = 1.0 slpm, a pressure of 8 Torr and an injected microwave power P_{MW} = 150 W, that previously allow obtaining high concentrations of active species in the late afterglows of N_2/He and N_2/H_2 mixtures [11].

TiO_2 samples can eventually be exposed (heated or not) in a 5 l Pyrex reactor following the afterglow quartz tube (results not shown in this paper).

Optical emission spectroscopy (OES) along the afterglow tubes was performed using an optical fibre connected to an Acton Spectra Pro 2500i spectrometer (grating 600 g/mm), equipped with a Pixis 256E CCD detector (front illuminated 1024 × 256 pixels).

Active Species Densities in R/2-10%(N_2–5%H_2) Afterglows (R = Ar or He)

Table 1 gathers the kinetic reactions used in this work, with the corresponding rate coefficients and their origin in the literature.

N-Atom, N_2(A), N_2^+ and N_2(X, v > 13) Densities

In flowing afterglows, absolute N atom densities can be obtained by NO titration, a method extensively described in [8–10, 22] and well suited to the study of N_2 late afterglows between 5 and 10 Torr. In this pressure range, a good agreement has been found for absolute N-atom densities measured using the NO titration method and using the non-intrusive TALIF (Two-photon Absorption Laser-Induced Fluorescence) method [23].

In full late afterglow conditions, the N_2 (1+) (11–7) band emission at 580 nm (I_{580}) is produced by the 3-body recombination process of N atoms:

$$\mathrm{N(^4S) + N(^4S) + M \rightarrow N_2(B, v' = 11) + M} \tag{a}$$

$$\mathrm{N_2(B, v' = 11) \rightarrow N_2(A, v'' = 7) + h\nu(1+,\ 580\ nm)} \tag{a'}$$

In the early afterglow, here defined as the afterglow region lying between the pink and the late afterglow, only a fraction (a_{N+N}, with $0 \le a_{N+N} \le 1$) of the I_{580} emission is due to the process (a), the remaining fraction being caused by collisions between high vibrationally excited levels of the ground molecular state N_2(X,v > 13) and metastable states N_2(A):

$$\mathrm{N_2(X, v > 13) + N_2(A) \rightarrow N_2(B, 0 \le v'' < 12) + N_2} \tag{b}$$

In consequence, in the early afterglow region and neglecting a possible quenching of the N_2(B,v′ = 11) level by H_2 molecules, the N atom concentration can be related to the a_{N+N} fraction of the observed I_{580} emission through the proportionality relation:

$$a_{N+N} I_{580} = k_1 [N]^2 \tag{1}$$

with $k_1 = c_{580} \frac{hc}{580} A_{A,7}^{B,11} \frac{k_a[M]}{\left(\upsilon^R_{N_2(B,11)} + [R]k^{Q_R}_{N_2(B,11)} + [N_2]k^{Q_{N_2}}_{N_2(B,11)}\right)}$ where $[M] = \frac{p}{kT} = 2.6 \times 10^{17}\ \mathrm{cm^{-3}}$ at p = 8 Torr and T = 300 K, c_{580} is the spectral response of the spectral intensity acquisition system at 580 nm, $A_{A,7}^{B,11}$ is the vibrational transition probability of the N_2(1+, 11–7) band,

Table 1 Kinetics reactions and corresponding rate coefficients in the R-N_2–H_2 afterglows

Reaction	Symbol	Rate coefficient	Reference
$N(^4S) + N(^4S) + M \rightarrow N_2(B, v'=11) + M$	k_a	Varying from 3×10^{-34} cm^6 s^{-1} for M = Ar–2%N_2 to 9×10^{-34} cm^6 s^{-1} for M = N_2	[8–10]
		4×10^{-34} cm^{6}s^{-1} for M = He/(5–40%)N_2	[11]
$N_2(B, v'=11) \rightarrow N_2(A, v''=7) + h\nu$ (1+, 580 nm)	$A^{B,11}_{A,7}$	7.8×10^4 s^{-1}	[8–10]
$N_2(B, v'=11) \rightarrow N_2(A) + h\nu$ (1+)	$\upsilon^R_{N_2(B,11)}$	2×10^5 s^{-1}	[8–11]
$N_2(B, v'=11) + N_2 \rightarrow N_2 + N_2$	$k^{Q_{N_2}}_{N_2(B,11)}$	3×10^{-11} cm^3 s^{-1}	[8–11]
$N_2(B, v'=11) + Ar \rightarrow N_2 + Ar$	$k^{Q_{Ar}}_{N_2(B,11)}$	0.2×10^{-11} cm^3 s^{-1}	[8–11]
$N_2(B, v'=11) + He \rightarrow N_2 + He$	$k^{Q_{He}}_{N_2(B,11)}$	10^{-12} cm^3 s^{-1}	[8–11]
$N_2(X, v > 13) + N_2(A) \rightarrow N_2(B, 0 \leq v'' < 12) + N_2$	k_b	4×10^{-11} cm^3 s^{-1}	[12]
$N_2(A) + N_2(A) \rightarrow N_2(C, v'=1) + N_2(X)$	k_c	4.1×10^{-11} cm^3 s^{-1}	[13]
$N_2(C, v'=1) \rightarrow N_2(B, v''=0) + h\nu$ (2+, 316 nm)	$A^{C,1}_{B,0}$	1.3×10^7 s^{-1}	[8–10]
$N_2(C, v'=1) \rightarrow N_2(B) + h\nu$ (2+)	$\upsilon^R_{N_2(C,1)}$	2.7×10^7 s^{-1}	[8–10]
$N_2(C, v'=1) + N_2 \rightarrow N_2 + N_2$	$k^{Q_{N_2}}_{N_2(C,1)}$	3×10^{-11} cm^3 s^{-1}	[8–10]
$N_2(C, v'=1) + Ar \rightarrow N_2 + Ar$	$k^{Q_{Ar}}_{N_2(C,1)}$	5×10^{-12} cm^3 s^{-1}	[8–10]
$N_2(C, v'=1) + He \rightarrow N_2 + He$	$k^{Q_{He}}_{N_2(C,1)}$	2×10^{-12} cm^3 s^{-1}	[14]
$N_2^+(X) + N_2(X, v > 13) \rightarrow N_2^+(B, v'=0) + N_2(X)$	k_d	1×10^{-11} cm^3 s^{-1}	[15]
$N_2^+(B, v'=0) \rightarrow N_2^+(X, v''=0) + h\nu$ (1−, 391 nm)	$A^{B,0}_{X,0}$	1.2×10^7 s^{-1}	[16]
$N_2^+(B, v'=0) \rightarrow N_2^+(X) + h\nu$ (1−)	$\upsilon^R_{N_2^+(B,0)}$	1.7×10^7 s^{-1}	[16]
$N_2^+ (B, v'=0) + N_2 \rightarrow N_2^+ + N_2$	$k^{Q_{N_2}}_{N_2^+(B,0)}$	8.8×10^{-10} cm^3 s^{-1}	[8–10]
$N_2^+ (B, v'=0) + Ar \rightarrow N_2^+ + Ar$	$k^{Q_{Ar}}_{N_2^+(B,0)}$	2×10^{-10} cm^3 s^{-1}	[17]
$N_2^+ (B, v'=0) + He \rightarrow N_2^+ + He$	$k^{Q_{He}}_{N_2^+(B,0)}$	3×10^{-11} cm^3 s^{-1}	[17]
$N_2(X, v > 13) + NH \rightarrow N_2 + NH(A, v'=0)$	k_e	5×10^{-11} cm^3 s^{-1} (see text)	[13, 18]
$NH(A, v'=0) \rightarrow NH(X, v''=0) + h\nu$ (336 nm)	$A^{A,0}_{X,0}$	2×10^6 s^{-1}	[19]
$NH(A, v'=0) \rightarrow NH(X) + h\nu$	$\upsilon^R_{NH(A,0)}$	2×10^6 s^{-1}	[19]
$NH(A, v'=0) + N_2 \rightarrow NH + N_2$	$k^{Q_{N_2}}_{NH(A,0)}$	$< 9 \times 10^{-14}$ cm^3 s^{-1}	[19]
$NH(A, v'=0) + Ar \rightarrow NH + Ar$	$k^{Q_{Ar}}_{NH(A,0)}$	$< 9 \times 10^{-14}$ cm^3 s^{-1}	[19]
$NH(A, v'=0) + He \rightarrow NH + He$	$k^{Q_{He}}_{NH(A,0)}$	$< 9 \times 10^{-14}$ cm^3 s^{-1}	[19]
$NH(A, v'=0) + H_2 \rightarrow NH + H_2$	$k^{Q_{H_2}}_{NH(A,0)}$	5×10^{-11} cm^3 s^{-1}	[19]
$N + H + M \rightarrow NH + M$	k_f	$5(\pm 3) \times 10^{-32}$ cm^6 s^{-1}	[20]
$N + NH \rightarrow H + N_2$	k_g	5×10^{-11} cm^3 s^{-1}	[21]

k_a is the rate coefficient for reaction (a), $\upsilon^R_{N_2(B,11)}$ and $k^{Q_i}_{N_2(B,11)}$ are respectively the radiative loss frequency and the quenching rates of the $N_2(B, v''=11)$ level by species i (i = R or N_2).

As reported by Ricard et al. [11, 13], the $N_2(A)$ and $N_2(X,v>13)$ densities can be deduced from the N-atom density by line ratio methods. Assuming that the following reation (c) is the dominant process for the production of the $N_2(C,v'=1)$ level:

$$N_2(A) + N_2(A) \rightarrow N_2(C, v' = 1) + N_2(X) \quad \text{(c)}$$

$$N_2(C, v' = 1) \rightarrow N_2(B, v'' = 0) + h\nu\,(2+,\ 316\ \text{nm}) \quad \text{(c')}$$

Using the same definitions than above, it comes for the I_{316} intensity:

$$I_{316} = k_2\left[N_2(A)\right]^2 \quad (2)$$

with $k_2 = c_{316}\frac{hc}{316}A_{B,0}^{C,1}\frac{k_c}{\left(\upsilon^R_{N_2(C,1)}+[R]k^{Q_R}_{N_2(C,1)}+[N_2]k^{Q_{N_2}}_{N_2(C,1)}\right)}$

The $N_2(A)$ density can then be deduced from the absolute [N] concentration and the measured $\frac{I_{580}}{I_{316}}$ band intensity ratio, following:

$$a_{N+N}\frac{I_{580}}{I_{316}} = k_3\left(\frac{[N]}{[N_2(A)]}\right)^2 \quad (3)$$

where $k_3 = \frac{k_1}{k_2} = 2.5(\pm 0.5)\times 10^{-7}$ in Ar/> 10%N_2 and He/> 10%N_2 and $k_3 = 4\times 10^{-7}$ in Ar/(2–5%)N_2, with $\frac{c_{580}}{c_{316}} = 7$ [8–10].

Assuming now that in the early afterglow, $N_2(B,v=11)$ levels can also be produced by reactions (b), it comes:

$$\frac{a_{N+N}}{1 - a_{N+N}} = k_4\frac{[N]^2}{\left([N_2(A)][N_2(X, v > 13)]\right)} \quad (4)$$

where $[N_2(X,v>13)]$ is the sum of the densities of the $N_2(X,v)$ vibrational levels conducing to the exothermicity of reaction (b), happening for v > 13. It is calculated $k_4 = \frac{k_1}{k_b} = 7\times 10^{-6}$ in Ar/> 2%N_2 and in He/> 80%N_2, slowly decreasing to $k_4 = 5\times 10^{-6}$ in He/(60–80%)N_2, $k_4 = 3\times 10^{-6}$ in He/(10–40%)N_2 and $k_4 = 2\times 10^{-6}$ in He/(2–5%)N_2.

Considering that the N_2^+ (1−) (0–0) band emission at 391 nm (I_{391}) is produced by the following processes:

$$N_2^+(X) + N_2(X, v > 13) \rightarrow N_2^+\left(B, v' = 0\right) + N_2(X) \quad \text{(d)}$$

$$N_2^+(B, v' = 0) \rightarrow N_2^+(X, v'' = 0) + h\nu\,(1-,\ 391\ \text{nm}), \quad \text{(d')}$$

the N_2^+ ion concentration can be deduced from the $\frac{I_{391}}{I_{316}}$ band intensity ratio, following the equation:

$$\frac{I_{391}}{I_{316}} = \frac{k_6}{k_2}\frac{\left[N_2^+\right]\left[N_2(X, v > 13)\right]}{\left[N_2(A)\right]^2} = k_5\frac{\left[N_2^+\right]\left[N_2(X, v > 13)\right]}{\left[N_2(A)\right]^2} \quad (5)$$

with $k_6 = c_{391}\frac{hc}{391}A_{X,0}^{B,0}\frac{k_d}{\left(\upsilon^R_{N_2^+(B,0)}+[R]k^{Q_R}_{N_2^+(B,0)}+[N_2]k^{Q_{N_2}}_{N_2^+(B,0)}\right)}$ k_5 is found to decrease from 8.5 to 4×10^{-2} in Ar/x%N_2 and from 12 to 4×10^{-2} in He/x%N_2 when x increases from 20 to 100% [11].

Uncertainties in species densities estimation by this line ratio methods are 30% for the N-atoms (only caused by errors made during NO titration, see for example the interesting discussion in [22]) and at least 50% for $N_2(A)$, where additional sources of errors are related to the determination of the a_{N+N} parameter and to uncertainties in the rate coefficients of Table 1. For $N_2(X,v>13)$ and N_2^+, only the order of magnitude is expected because of the uncertainty increase linked to the use of the $\frac{a_{N+N}}{1-a_{N+N}}$ ratio.

NH Radical and H-Atom Densities

As previously stated in [8–10], it is estimated that the NH(A,v=0) radiative state is produced by the exothermic reaction (e), due to the endothermicity of the 3 body recombination N+H+M→NH(A,v=0)+M:

$$N_2(X,v>13) + NH \rightarrow N_2 + NH(A,v=0) \tag{e}$$

$$NH(A,v=0) \rightarrow NH(X,v=0) + h\nu(336\ nm) \tag{e'}$$

The intensity ratio method above developed can be applied to determine the absolute NH radical density, conducing to:

$$I_{336} = k_7[NH]\left[N_2(X,v>13)\right] \tag{6}$$

with $k_7 = c_{336}\frac{hc}{336}A_{X,0}^{A,0}\frac{k_e}{\left(\upsilon^R_{NH(A,0)}+[R]k^{Q_R}_{NH(A,0)}+[N_2]k^{Q_{N_2}}_{NH(A,0)}\right)}$

$$a_{N+N}\frac{I_{580}}{I_{336}} = \frac{k_1}{k_7}\frac{[N]^2}{\left([NH][N_2(X,v>13)]\right)} = k_8\frac{[N]^2}{\left([NH][N_2(X,v>13)]\right)}. \tag{7}$$

Using $\frac{c_{580}}{c_{336}}=5$ [8–10], $A_{X,0}^{A,0} = \upsilon^R_{NH(A,0)}$ and $k_e=5\times10^{-11}$ cm^3 s^{-1} (chosen to be equal to the rates of the $N_2(X,v>13)+N_2(A)\rightarrow N_2+N_2(B,11)$ and $N_2(X,v>13)+N_2^+\rightarrow N_2+N_2^+(B)$ exothermic reactions [13, 18]), it is calculated $k_8=1.3\times10^{-7}$ in pure N_2 and in Ar/>40%N_2, $k_8=3.0\times10^{-7}$ in Ar/<40%N_2 and $k_8=2.0\ (\pm0.5)\times10^{-7}$ in He/>2%N_2.

The H-atom and NH radical densities are related by the following kinetics:

$$N + H + M \rightarrow NH + M \tag{f}$$

$$N + NH \rightarrow H + N_2 \tag{g}$$

Using the pseudo-stationary approximation and considering the k_f rate coefficient independent of the third body ($k_f^{N_2} = k_f^{Ar} = k_f^{He}$), it comes at 8 Torr:

$$[NH] = \frac{k_f}{k_g}[H][M] = 2.610^{-4}[H] \tag{8}$$

Figure 2 reproduces spectra measured at z=3 cm in the Ar/2%(N_2–5%H_2) mixture at 8 Torr, 1 slpm and 150 W.

In Fig. 2a, the NH (0–0) and (1–1) bands at respectively 336 and 337 nm are the most intense emissions. It is also observed the N_2 2+ (1–0) band at 316 nm, the NO β (0–8) band at 320 nm and the N_2^+ (0–0) band at 391 nm, close to the CN violet bands between 385 and 388 nm. For data treatment, the NH (1–1) band at 337 nm has been discarded

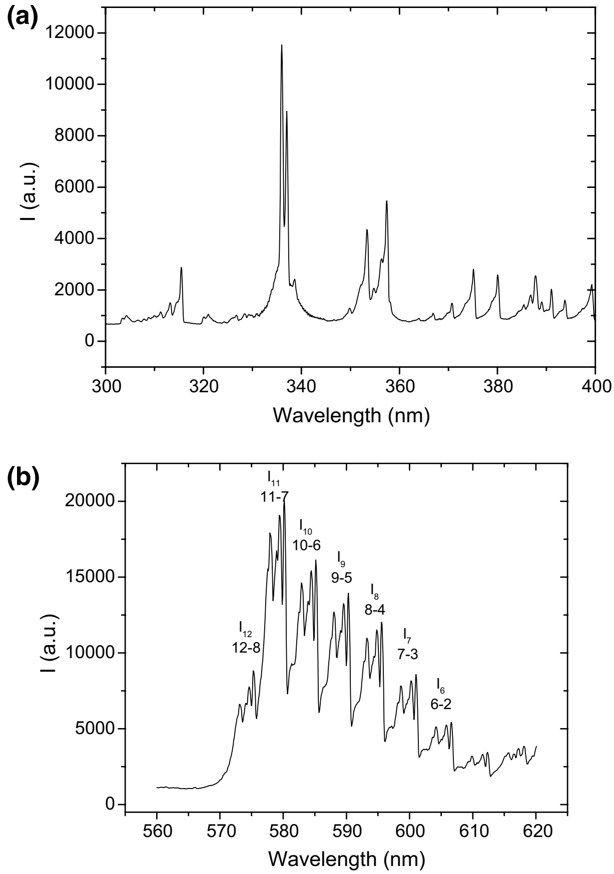

Fig. 2 **a** Sequence 300–400 nm, **b** sequence 560–620 nm of the N_2 1+ system observed in the Ar/2%(N_2–5%H_2) afterglow at z = 3 cm. (8 Torr, 1 slpm, 150 W, 1 ms)

because of possible mixing with the N_2 2+ (0–0) band at 337 nm. The I_{336} intensity is thus measured from the half intensity of the I_{336} and I_{337} band junction.

As previously shown by considering the I_{11}/I_9 ratio, the a_{N+N} coefficient can be deduced from the vibrational distribution observed in Fig. 2b [11]. With the experimental conditions of Fig. 2, it is found the value $a_{N+N} = 0.35$ and after calibration by NO titration, it is deduced $[N] = 1.0 \times 10^{15}$ cm^{-3}.

In previous studies [11], the NH and H densities were obtained in N_2/2.5%H_2, Ar/50%(N_2–5%H_2) and He/80%(N_2–5%H_2) gas mixtures. For N_2/2.5%H_2 and Ar/50%(N_2–5%H_2), it was found a $[H]/2[H_2]$ dissociation rate of about 0.3%. In the He/80%(N_2–5%H_2) mixture, the hydrogen dissociation rate was found to be higher (1.0%) and it was obtained a [H]/[N] ratio of about 30%.

According to Eq. (7), the accuracy of the determination of the [NH] density largely depends on the accuracy of the $[N_2(X,v>13)]$ density (limited to the order of magnitude) and on the choice of the k_e rate coefficient for reaction (e), chosen to be similar to the one of the $N_2(X,v>13) + N_2(A) \rightarrow N_2 + N_2(B,11)$ and $N_2(X,v>13) + N_2^+ \rightarrow N_2 + N_2^+(B)$ exothermic reactions [11].

As the H density is related to the NH density through Eq. (8) and to the k_f rate coefficients of the 3-body recombination $N + H + M \rightarrow NH + M$, it is clear that the presented absolute densities of NH radicals and H atoms are highly speculative. Nevertheless, their relative variations with R(He or Ar) and with the dilution x of the (N_2–5%H_2) mixture in the rare gas remain significant.

Table 2 compares the a_{N+N} coefficients and the absolute densities obtained at z = 3 cm using the developed line ratio methods in the He/x(N_2–5%H_2) and the Ar/x(N_2–5%H_2) mixtures, for x varying between 2 and 10% (8 Torr, 1 slpm, 150 Watt).

With He and for x < 20%, the accuracy of the abacus given in Fig. 3a [7] and showing the variation of the I_{11}/I_9 ratio is too low and it has been chosen to use instead the I_{11}/I_{10} ratio, given in Fig. 3b.

At high dilutions (2% and 5%), N-atom, $N_2(A)$, N_2^+ and $N_2(X,v > 13)$ densities are higher in Ar/x(N_2–5%H_2) mixtures than in He/x(N_2–5%H_2) mixtures. At lower dilutions (20–50%), densities of N_2^+ and $N_2(X,v > 13)$ are also higher in the Ar mixture than in the He mixture.

Whatever the buffer gas (R = Ar or He), nitrogen and hydrogen dissociation rates are the highest in highly diluted mixtures (x = 2%). The nitrogen dissociation rate, which is usually less than 1% in pure N_2 afterglows [8–10], increases by one order of magnitude with high dilution in Ar, to reach 10% in the Ar/2%(N_2–5%H_2) mixture.

The H-atom concentration is minimum in medium dilution mixtures (5–10%), while the N-atom concentration is less dilution dependent. As produced by the 3-body reaction (f), the NH density also shows a minimum for (5–10%) mixtures.

Table 2 a_{N+N} coefficients, active species densities and dissociation rates determined at z = 3 cm in the early afterglows of R/x%(N_2–5%H_2) gas mixtures for x = 2–10% (8 Torr, 1 slpm and 150 W)

	R/x(N_2–5%H_2)	2%	5%	10%	20%	40%	50%
a_{N+N}	R = He	0.6[a]	0.3[a]	1.0–0.3[a]	0.7	0.45–0.8[a]	0.7
	R = Ar	0.35	0.6	0.7	0.9		
[N]	R = He	0.8[a]	0.7[a]	1.5–1.2[a]	1.2	1.0–0.7[a]	2.0
(10^{15} cm^{-3})	R = Ar	1.0	2.2	1.1	2.6		
[N_2(A)]	R = He	2.3[a]	2.5[a]	2–3[a]	2.2	2.0–1.1[a]	2.0
(10^{11} cm^{-3})	R = Ar	4.0	3.5	1.0	7.0		
[$N_2(X,v > 13)$]	R = He	0.5[a]	1.4[a]	3.5[a]	0.8	2.0–0.3[a]	5.0
(10^{13} cm^{-3})	R = Ar	3.0	6.4	3.6	1.7		
[N_2^+]	R = He	1.3[a]	0.4[a]	0.4[a]	1.0	0.2	1.5
(10^{10} cm^{-3})	R = Ar	2.0	0.9	1.0	7.0		
[NH]	R = He	0.7[a]	0.3[a]	0.3[a]	1.0	0.3–0.8[a]	3.5
(10^{10} cm^{-3})	R = Ar	2.0	0.1	0.04	0.3		
[H]	R = He	3.0[a]	1.0[a]	1.0[a]	4.0	1–3[a]	13
(10^{13} cm^{-3})	R = Ar	8.0	0.4	0.2	1.0		
[H]/2[H_2]	R = He	6[a]	0.8[a]	0.4[a]	0.8	0.1–0.3[a]	1
(%)	R = Ar	15	0.3	0.08	0.2		
[N]/2[N_2]	R = He	8[a]	3[a]	2[a]	1.0	0.5	0.5
(%)	R = Ar	10	9	2	2.5		

The [NH] and [H] densities are calculated with $N_2(X,v > 13)$ + NH and N + H + M rate coefficients of 5×10^{-11} cm^3 s^{-1} and 5×10^{-32} cm^6 s^{-1}

[a] a_{N+N} calculated from I_{11}/I_{10} (Fig. 3b)

Fig. 3 Variation of the I_{11}/I_9 (**a**) and I_{11}/I_{10} (**b**) band intensity ratios in the mixed region between the pink afterglow ($a_{N+N}=0$) and the full late afterglow ($a_{N+N}=1$) for the He/x(N_2–5%H_2) mixtures, with x=2–100% (Color figure online)

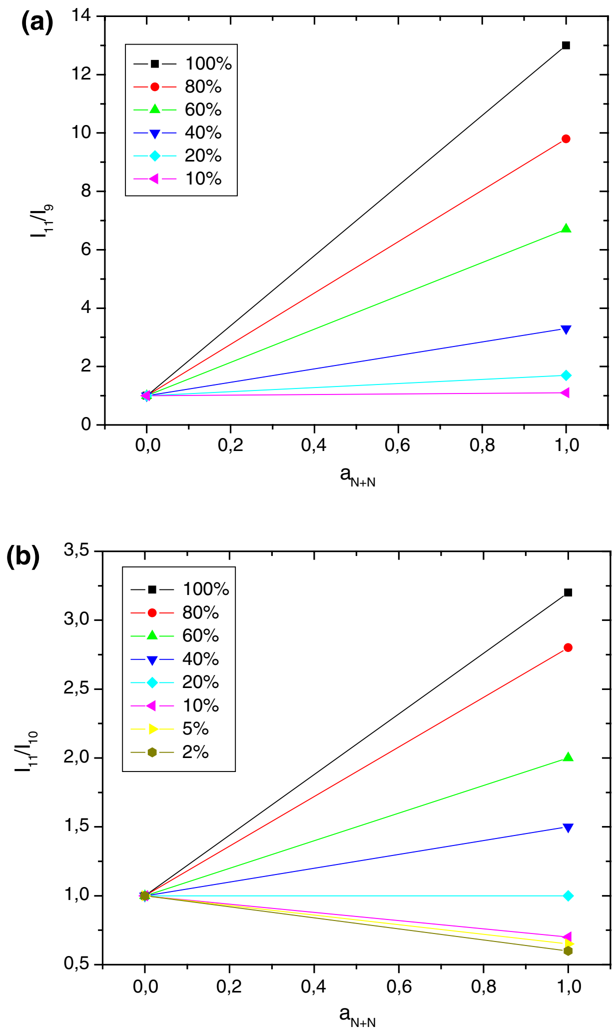

Destruction of H-Atoms on the Quartz Tube Wall

From values reported in Table 3 for the Ar/2%(N_2–5%H_2) afterglow, it is deduced that the N–atom density remains practically constant along the dia.18 mm quartz afterglow tube between 3 and 35 cm (10^{-3} to 10^{-2} s). At the contrary, the H-atom density shows a sensitive decrease, which is the result of a significant destruction on the tube wall.

Assuming that at 8 Torr, H-atoms losses in the afterglow are only due to wall recombination through $H+H+wall \rightarrow H_2+wall$ and $H+N+wall \rightarrow NH+wall$ processes, the global γ_H destruction probability on the quartz tube walls can be calculated, as demonstrated in [2] for the N atoms. It is written:

$$[H]_z = [H]_{z=0} exp\left[-\frac{\nu_H z}{v}\right] \quad (8)$$

Table 3 a_{N+N} factors (from the $I_{11/9}$ band ratio) and active species densities determined at z = 3, 25 and 35 cm in the afterglows of an Ar/2%(N_2–5%H_2) gas mixture (8 Torr, 1 slpm and 150 W)

	Ar/2%(N_2–5%H_2)		
z (cm)	3	25	35
a_{N+N}	0.4	0.6	0.6
[N] (10^{15} cm^{-3})	1	0.8	0.8
[N_2(X,v > 13)] (10^{13} cm^{-3})	3	5.5	5.3
[NH] (10^9 cm^{-3})	20	0.1	0.04
[H] (10^{13} cm^{-3})	8	0.04	0.01
[H]/2[H_2] (%)	15	0.08	0.02
γ_H^{Ar} (10^{-3})	4.0		

The γ_H^{Ar} value is calculated from the [H] density variation between 3 and 35 cm

with $\nu_H = \gamma_H \frac{\langle v \rangle}{2r}$, where $\langle v \rangle$ is the thermal gas velocity ($\langle v \rangle = 5 \times 10^4$ cm s^{-1} at 300 K) and r is the tube radius

z = 0 being taken at the beginning of the afterglow in the dia.18 mm tube (Fig. 1), it is obtained $\gamma_H^{Ar} = 4 \times 10^{-3}$

As reported in Table 4 for 2% ≤ x ≤ 10% in He/x(N_2–5%H_2) mixtures, the N-atom density also shows a nearly constant value between the early and the late afterglow.

[N_2(A)] and [N_2^+] densities decrease sharply between z = 3 cm and z = 40 cm while the [N_2(X,v > 13)] density increases. The high concentrations of [N_2(X,v > 13)] obtained for

Table 4 a_{N+N} factors (from the $I_{11/10}$ band ratio) and active species densities determined at z = 3, 20 and 40 cm in the afterglows of He/x%(N_2–5%H_2) gas mixtures with x = 2, 5 and 10% (8 Torr, 1 slpm and 150 W)

He/x(N_2–5%H_2)	x = 2%			x = 5%			x = 10%		
z (cm)	3	20	40	3	20	40	3	20	40
a_{N+N}	0.6	0.6	0.7	0.3	0.4	0.5	0.3	0.2	0.4
[N] (10^{15} cm^{-3})	0.8	0.9	0.8	0.7	0.9	0.8	1.2	1.3	1.0
[N_2(A)] (10^{11} cm^{-3})	2.3	0.7	0.25	2.5	0.8	0.3	3.0	1.6	0.4
[N_2(X,v > 13)] (10^{13} cm^{-3})	0.5	2.0	3.3	1.4	4.5	6.4	3.5	13	11
[N_2^+] (10^9 cm^{-3})	13	0.4	0.09	4	0.3	0.06	4.0	0.35	0.07
[NH] (10^9 cm^{-3})	7.0	0.2	0.04	3.0	0.15	0.03	3.0	0.3	0.03
[H] (10^{13} cm^{-3})	3	0.08	0.02	1.0	0.06	0.01	1.0	0.12	0.01
[H]/2[H_2] (%)	6	0.15	0.04	0.8	0.05	0.01	0.4	0.05	0.004
γ_H^{He} (10^{-4})	2.0			2.0			2.5		

γ_H^{He} values are calculated from [H] density variations between 3 and 40 cm

$z \geq 20$ cm are related to low densities of [N_2(A)], resulting of dominant loss frequencies of N_2(X,v > 13) and N_2(A) densities produced by reaction (b) where $k_b = 4 \times 10^{-11}$ cm^3 s^{-1} [12].

Using Eq. (8), a global destruction probability of $\gamma_H^{He} = 2.5(\pm 1.0) \times 10^{-4}$ is obtained in He/x(N_2–5%H_2) mixtures. It has been observed that γ_H^{He} kept a nearly constant value for x = 2–90%. The obtained order of magnitude is in good agreement with values $\gamma_H^{H_2} = 7 \times 10^{-4}$ and $\gamma_H^{N_2/H_2} = 4 \times 10^{-4}$ previously reported in H_2 and a N_2–90%H_2 gas mixture [24]. It appears that the γ_H^{Ar} value in the Ar/2%(N_2–5%H_2) gas mixtures is higher by about one order of magnitude. In comparison, the $\gamma_N^{N_2}$ value of the N-atoms destruction probability on quartz walls in pure N_2 is in the range 10^{-5}–10^{-4} [2, 23], decreased by a factor 2 when 1% H_2 is introduced into N_2 [24].

The $\gamma_N^{N_2}$ value is thus about one order of magnitude lower than γ_H^{He} and two orders of magnitude lower than γ_H^{Ar}.

Conclusion

Early afterglows of R/x%(N_2–5%H_2) (R = Ar or He) gas mixtures have been studied to obtain the absolute densities of N-atoms, N_2(A) and N_2(X,v > 13) metastable molecules by line intensity ratio methods, after calibration of the N-atom density by NO titration. The line intensity ratio method also allowed estimating the density of NH radicals and H-atoms.

For this evaluation, a rate coefficient of 5×10^{-11} cm^3 s^{-1} has been considered for the reaction N_2(X,v > 13) + NH → N_2 + NH(A,v = 0) and a rate coefficient of 5×10^{-32} cm^6 s^{-1} for the N + H + M → NH + M 3-body recombination.

Such values conduce to high dissociation rates of H_2 and N_2 in R/x%(N_2–5%H_2) early afterglows with R = Ar or He ([H]/2[H_2] = 15% with Argon and 6% with He) for x < 5% at 8 Torr, 1 slpm, 150 W.

Using H-atoms density profiles along the afterglow quartz tubes, the global H-atom destruction probability γ_H^R was calculated in the different R/x%(N_2–5%H_2) gas mixtures.

It is found a value $\gamma_H^{He} = 2.5(\pm 1.0) \times 10^{-4}$ in the He/(2–90)%(N_2–5%H_2) mixtures, one order of magnitude lower than the $\gamma_H^{Ar} = 4 \times 10^{-3}$ value obtained in the Ar/2%(N_2–5%H_2) mixture. The γ_H^{He} probability is in good agreement with data published by Gordiets et al. and is higher by one order of magnitude when compared with the $\gamma_N^{N_2}$ recombination probability.

Appearing to be a rich source of NH radicals and H atoms, accompanying dominant N-atoms, highly diluted R/2%(N_2–5%H_2) (R = Ar or He) early afterglows are of interest for surface treatments, as already observed for selective surface nitriding of TiO_2 films [3, 4] in pure N_2 afterglow.

In future works, the N and H atoms absolute densities will be determined by TALIF to compare with the present results obtained by NO titration and the line-ratio intensity method.

References

1. Villeger S, Sarrette JP, Ricard A (2005) Plasma Process Polym 2:709
2. Villeger S, Sarrette JP, Rouffet B, Cousty S, Ricard A (2008) Eur Phys J Appl Phys 42:25
3. Ryu S, Wang Y, Ricard A, Sarrette JP, Kim A, Kim A, Kim YK (2019) Accepted Surf Coat Technol
4. Wang Y, Ricard A, Sarrette JP, Kim A, Kim YK (2017) Surf Coat Technol 324:243

5. Ferreira JA, Nguyen HTP, Mi Z, Leonelli R, Stafford L (2014) Nanotechnology 25:435606
6. Bigras GR, Glad X, Martel R, Sarkissian A, Stafford L (2018) Plasma Sources Sci Technol 27:124004
7. Bigras GR, Glad X, Vandsburger L, Charpin C, Levesque P, Martel R, Stafford L (2019) Carbon 144:532
8. Zerrouki H, Ricard A, Sarrette JP (2013) Contrib Plasma Phys 53:599
9. Zerrouki H, Ricard A, Sarrette JP (2014) Contrib Plasma Phys 54:827
10. Zerrouki H, Ricard A, Sarrette JP (2014) J Phys Conf Ser 550:012045
11. Ricard A, Sarrette JP (2019) J Phys Conf Ser. **(accepted for publication)**
12. Piper LG (1994) J Chem Phys 101:10229
13. Ricard A, Oh SG, Guerra V (2013) Plasma Sources Sci Technol 22:035009
14. Gat E, Gherardi N, Lemoing S, Massines F, Ricard A (1999) Chem Phys Lett 306:263
15. Anketell J (1977) Can J Phys 55:1134
16. Laux CO, Kruger CH (1992) JQSRT 48:9
17. Tellinghuisen JB, Winkler CA, Freeman CG, McEwan MJ, Phillips LF (1972) J Chem Soc Faraday Trans II 68:833
18. Ricard A, Oh SG (2014) Plasma Sources Sci Technol 23:045009
19. Hofzumahaus A, Stuhl F (1985) J Chem Phys 82:3152
20. Brown RL (1973) Int J Chem Kinet 5:663
21. Tatarova E, Dias FM, Gordiets B, Ferreira CM (2005) Plasma Sources Sci Technol 14:19
22. Vasina P, Kudrle V, Talsky A, Botos P, Mrazkova M, Mesko M (2004) Plasma Sources Sci Technol 13:668
23. Rouffet B, Gaboriau F, Sarrette JP (2010) J Phys D Appl Phys 43:185203
24. Gordiets B, Ferreira CM, Pinheiro MJ, Ricard A (1998) Plasmas Sources Sci Technol 7:363